

# Probing Chemical and Mechanical Nanodomains in Copolymer Nanorods with Correlative Atomic Force Microscopy—Nano-correscopy

Dipesh Khanal, Bokai Zhang, Iqbal Ramzan, Curtis Marcott, Quan Li, and Wojciech Chrzanowski\*

The interplay between size, shape, mechanical properties, and surface chemistry of nanoparticles orchestrates cellular internalization, toxicity, circulation time, and biodistribution. Therefore, the safety of nanoparticles hinges on our ability to quantify nanoscale physicochemical characteristics. Current characterization tools, due to their limited resolution, are unable to map these properties correlatively at nanoscale. An innovative use of atomic force microscopy-based techniques, namely nano-correscopy, overcomes this limitation and offers multiprobe capability to map mechanical (viscous and elastic) and chemical domains of nanoparticles correlatively. The strengths of this approach are demonstrated using polymer composite nanorods: m-PEG-PLGA ((m-PEG–methoxy-poly (ethylene glycol)-*b*-poly (lactic-*co*-glycolic acid)). Precise distribution of PLGA (monomers of lactide and glycolide) and poly(ethylene glycol) (PEG) polymer across nanorods is identified. The hydrophobic lactide component is found predominantly at the apex, while hydrophilic glycolide and PEG assembled at the body of the nanorods and correlate with a gradient of nanomechanical properties. New knowledge of how both nanochemical domains and nanomechanical properties are distributed across the nanorod will allow elucidating the interactions of nanorods with the proteins and biomolecules in the future, which will directly influence the fate of nanorods in vivo and will guide new synthesis methods.


Physicochemical characteristics are central to the development of new nanomaterials for energy and environment, communication, computing, and security as well as health and medicine. While all these areas are of significant importance, health and medical applications remain the most chal-

lenging because they involve interactions with living organisms. Inherently such interactions are less predictable and are directly linked to human health, which highlight their societal impact. Therefore, resolving the principles that govern biological behaviors and developing modern technologies including nanomaterials are likely to result in significant advances in a search for new effective therapies for major health conditions such as cancer, diabetes, and infectious diseases. However, the emergence of nanomaterials of which properties are not well understood requires new methodologies to probe and characterize them at significantly greater resolution and more precisely than what is offered by traditional approaches. Here, we present a new approach for correlative nanoscopy capable of probing physicochemical properties. This approach characterizes with ultrahigh resolution and correlation of physical and chemical channels. We demonstrated its strengths and capabilities based on hypothetical biomedical applications of our test samples.

In the last decade, nanotechnology and new polymerization methods have revolutionized the biomedical field, providing new opportunities to manufacture nanoparticle-based systems for more effective drug delivery, bioimaging, and biosensing. For example, controlled radical polymerization and ring opening metathesis polymerization enable the manufacturing of nanoparticles with tunable rigidity (stiffness),

D. Khanal, Prof. I. Ramzan, Prof. W. Chrzanowski  
Faculty of Pharmacy  
The University of Sydney  
NSW 2006, Australia  
E-mail: wojciech.chrzanowski@sydney.edu.au

Dr. B. Zhang, Prof. Q. Li  
Department of Physics and Centre for Quantum Coherence  
The Chinese University of Hong Kong  
Shatin, New Territories 999077, Hong Kong

 The ORCID identification number(s) for the author(s) of this article can be found under <https://doi.org/10.1002/ppsc.201700409>.

Prof. C. Marcott  
Light Light Solutions  
P. O. Box 81486, Athens, GA 30608-1484, USA  
Prof. W. Chrzanowski  
University of Sydney Nano Science Institute  
The University of Sydney  
NSW 2006, Australia

DOI: 10.1002/ppsc.201700409

shape, and chemistry (e.g. monomer sequencing).<sup>[1]</sup> By controlling spatial distribution of individual building blocks of nanoparticle assembly, it is possible to modulate nanoparticle internalization by cells, circulation time, biodistribution, and tissue targeting.<sup>[2]</sup> But how these elaborate nanoscale structures control biological responses is currently poorly understood due to the recent emergence of nanomaterials and the limited spatial resolution of conventional characterization methods. Precise knowledge of the chemical and physical characteristics of nanoparticles will ultimately allow us to predict their safety and fate in biological systems and in the environment. It will unlock new opportunities to create safe-by-design systems for various biomedical applications.<sup>[2]</sup>

It is recognized that there is no single parameter which controls all biological responses. Rather, it is the interplay of many parameters such as size, shape, surface charge, chemistry, and mechanical properties that defines the final outcome. Therefore, correlative characterization of physical and chemical properties at the nanoscale is paramount in order to correlate nanoparticle structure to its function.

One class of nanoparticles that has attracted increasing attention but their interactions in bodily environment are not fully elucidated is elongated nanoparticles (rod-shape and needle-shape). Recent studies emphasized that these nanoparticles may offer advantages over spherical nanoparticles, in particular for specific therapeutic applications such as cancer drug delivery, where enhanced penetration into the nucleus was achieved.<sup>[3,4]</sup> However, these benefits depend strongly on the chemical composition and mechanical properties (rigidity and stiffness),<sup>[4,5]</sup> which can be modified using a combination of two or more polymers.<sup>[1,6]</sup>

Although there has been rapid progress in the synthesis of composite nanoparticles, characterization is still predominantly done using conventional methods that have limited resolution and were developed for bulk materials.<sup>[7]</sup> X-ray diffraction, scanning electron microscopy, transmission electron microscopy, small angle X-ray scattering, energy dispersive analysis of X-rays, electron energy loss spectroscopy, X-ray photoelectron spectroscopy, and time-of-flight secondary-ion mass spectrometry are some of the widely used tools to assess the chemical properties of nanoparticles.<sup>[8]</sup> However, these techniques only produce an averaged measurement of the specific character of the nanoparticles. Other commonly used techniques include Fourier transform infrared, Raman, and confocal Raman spectrophotometry. With lateral resolutions of 3 to 30  $\mu\text{m}$ ,<sup>[9,10]</sup> these techniques are unable to identify nanoscale differences within copolymer nanoparticles.

These limitations can be overcome with the use of a hybrid technique, which combines the high spatial resolution of atomic force microscopy (AFM) with infrared (IR) spectroscopy to achieve resolutions well below the diffraction limit of IR spectroscopy. The AFM-IR technique, which is also often referred to a photothermal induced resonance, enabled the evaluation of nanoscale chemical composition of bacteria with a resolution  $<20$  nm.<sup>[10-12]</sup> This detailed and precise understanding of nanoscale composition of bacteria would not have been possible with conventional FTIR and other techniques currently used, which further highlight capability and uniqueness of the AFM-IR technique. In addition, the contact resonance

frequency of the cantilever oscillation recorded during the spectra acquisition corresponds to the nanomechanical properties and helps to localize domains of different stiffness within the specimen.<sup>[12,13]</sup> AFM-IR offers correlative measurements of mechanical properties and chemical composition simultaneously, which add to its advantages.

In terms of mechanical properties characterization, conventional approaches such as acoustic impedance, spherical indentation, and nanoindentation are also suitable only for larger particles and simply cannot determine the nanomechanical domain with a resolution  $<20$  nm.<sup>[14,15]</sup> To address these limitations, a number of advanced AFM modes have been developed such as the amplitude modulation-frequency modulation atomic force microscopy,<sup>[16]</sup> force modulation, friction force microscopy, and contact resonance microscopic techniques such as piezoresponse microscopy<sup>[17]</sup> and atomic force acoustic microscopy.<sup>[18]</sup> Unfortunately, these modes themselves also have their own limitations. For example, the use of piezoelectric or ultrasonic forces in piezoresponse and atomic force acoustic microscopy introduces parasitic peaks from the false resonance of the piezo itself, which creates artifacts in the results. In addition, piezoresponse force microscopy is extremely specific and is only suitable for “harder” samples such as piezocrystals and ferroelectric material, which significantly limit its application.<sup>[17]</sup>

A promising new approach for mapping nanomechanical properties is the use of Lorentz contact resonance (LCR) spectroscopy. In LCR, the actuation of the cantilever is achieved with an oscillating Lorentzian force (**Figure 1b**) and it is not sample specific.<sup>[15,19-21]</sup> The sample is characterized based on the force modulation and the detection of changes to the cantilever deflection (frequency and amplitude), which directly correlate with viscous and elastic properties.<sup>[22]</sup> The advantage of LCR over conventional AFM techniques derives from the fact that the nanomechanical properties are mapped with nanometer resolution and the recorded signal comes from a thin, sub-surface layer, typically less than 20–60 nm. Therefore, substrate (here prism) stiffness has negligible influence on measured viscoelasticity, in particular for particles of high  $>200$  nm. Unlike other techniques (e.g., indentation), LCR uniquely provides a measure of elastic and viscous properties based on the frequency and amplitude of recorded signal.<sup>[15]</sup> Indentation-based methods enable only the calculation of apparent elastic moduli, which is influenced by the elastic component at different levels. These attributes make LCR one of the most suitable techniques for the qualitative and semiquantitative assessments of the distribution of viscoelasticity across the copolymeric particles.

The characterization of individual nanoparticles requires not only ultrasensitivity and accuracy, but also submicron resolution, which can be achieved with correlative use of different AFM modes. The combination of atomic force microscopy and infrared spectroscopy (AFM-IR) (**Figure 1a**), LCR (**Figure 1b**), and molecular force probe spectroscopy (MFP) (**Figure 1c**) offers the unprecedented resolution and sensitivity in mapping nanochemical and mechanical domains of individual nanoparticles.

In summary, interplay between physical and chemical properties of nanoparticles defines the fate of nanoparticles in biological systems. These parameters control cellular internalization, toxicity, circulation time, and biodistribution as well as

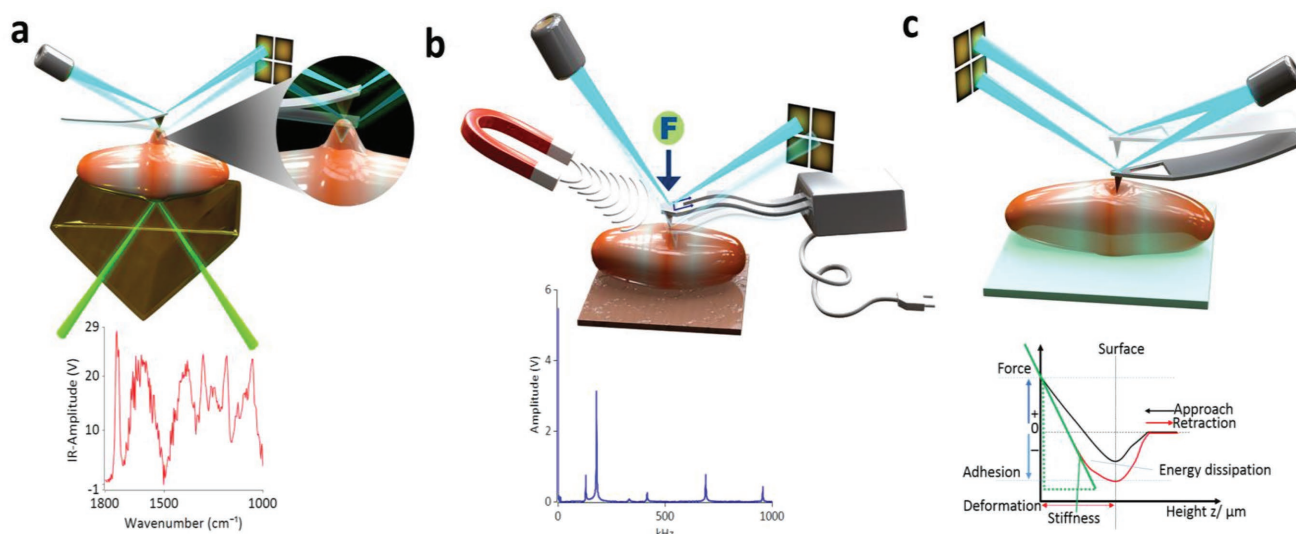


**Figure 1.** Schematic representation of nano-correscopy: a) Evaluation of chemical domains in a copolymeric nanorod with the use of AFM–IR technique; the corresponding AFM–IR spectra are presented, which precisely depict the chemical information at nanoscale. b) Identifying the viscoelastic domains within the nanorod with the Lorentz contact resonance spectroscopy technique, with the corresponding LCR spectra, where frequency corresponds to the stiffness and the amplitude of the peak indicates the viscosity. c) Quantifying the apparent elastic modulus of the nanorod with molecular force probe spectroscopy, after fitting the representative force volume curve apparent modulus at different regions of the sample can be obtained.

degradation rate. Since all these characteristics are interrelated, single technique or single end-point assay does not provide sufficient confidence to fully elucidate the suitability of nanoparticles for specific application or their safety. To address a significant gap in our capability to correlate between structure and properties, in particular to create “one-to-one” match, we introduce nano-correscopy that combines MFP microscopy, LCR spectroscopy for investigating nanomechanical properties (i.e., viscoelasticity), and AFM–IR for investigating the nano-chemical domains. To demonstrate strength of our approach that allowed ultrahigh resolution and correlative mapping of chemical and mechanical properties, we conducted a case study using rod-shape methoxy-poly (ethylene glycol)-*b*-poly (lactic-co-glycolic) acid–poly(ethylene glycol) (PLGA–PEG) composite nanoparticles.

Elongated needle- or rod-shaped copolymer nanoparticles, which can be used to tune stiffness and rigidity, are an emerging class of nanomaterials for drug delivery. Shape and stiffness of nanoparticles are becoming increasingly recognized as a key material parameter that orchestrates cellular internalization of nanoparticles and their toxicity. To tune the stiffness, polymers of different rigidity can be assembled to form an elongated composite structure. The reproducibility of the stiffness hinges on correct, well-controlled, sandwich-like assembly of polymer blocks. Theoretically, modern synthesis methods allow a uniform or gradual assembly. However, conventional characterization tools have limited capability and resolution to provide robust evidence of the nanoscale distribution of chemical domains and nanomechanical properties. Since such information is critical to understand and predict the interactions and degradation of the nanoparticles in biological systems, new characterization approaches that bring together and correlate the physical, chemical, and biological tools are needed. Our proposed approach, nano-correscopy, addresses precisely this

gap. The introduction of nano-correscopy is significant because it has the power to provide a fundamental understanding of how nanoparticles are assembled. This knowledge will guide future synthesis methods to align with “safe by design” strategy. It will allow better understanding of nanoparticle interactions with biological structures, including their degradation, which will enable the development of more effective and safe drug delivery systems or biosensors. It will also provide fundamental mechanistic insights into nanotoxicity to establish novel protocols for nanotoxicity testing to support regulatory agencies in protecting our health.

To demonstrate the capability of nano-correscopy in mapping chemical and physical characteristics, we used rod-shaped copolymer nanoparticle assemblies of m-PEG–PLGA with an average length of 1700 nm, width of 600 nm, and height of 280 nm as a model (Figure 2; Figures S2 and S3, Supporting Information).

An AFM–IR spectral array (Figure 2a) collected from the apex to the body of the nanorod with step of 150 nm showed significant differences in the distribution of chemical domains along the nanorod.

Interestingly, the intensity of peaks at 1740  $\text{cm}^{-1}$  associated with carbonyl ( $\text{C}=\text{O}$ ) stretching vibration of ester from PLGA and 1184  $\text{cm}^{-1}$  due to  $\text{C}-\text{C}-\text{O}$  stretching of ester, and 1384  $\text{cm}^{-1}$  due to  $\text{C}-\text{H}_3$  bending vibration<sup>[23–25]</sup> was found to be significantly stronger at the apex of the nanorod compared to the other regions (Figure 2a). In addition, the intensity of these ester peaks decreased significantly, when the spectra were collected away from the apex toward the body of the nanorod highlighting the existence of gradient regions with the mixture of both monomers of lactide and glycolide from PLGA. PLGA contains the monomers of hydrophobic lactide and hydrophilic glycolide units. Higher intensity of lactide monomeric unit at the apex of the nanorod indicated that these particles



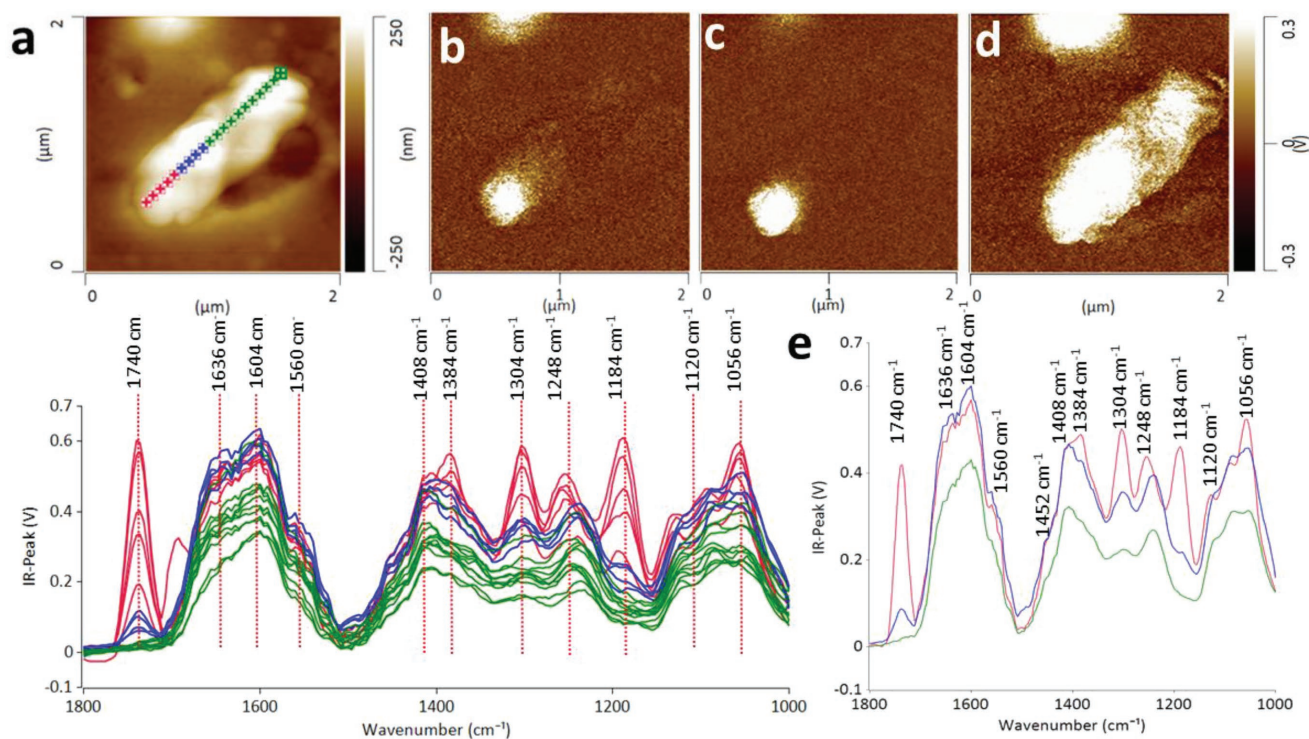


**Figure 2.** a) AFM–height image along with the AFM–IR spectral array collected from nanorods. The PLGA–ester peak was observed at 1740 and 1184  $\text{cm}^{-1}$  at the apex of the nanorod, indicating an ester rich domain along the tip of the nanorod. The intensity of ester rich domains decreased as the spectra were collected from closer proximity of the body of the nanorod. b, c) AFM–IR absorbance map ( $2 \mu\text{m} \times 2 \mu\text{m}$ ) collected at 1740 and 1184  $\text{cm}^{-1}$  showed the distribution of ester rich regions seen as bright white spots at the apex of the nanorod. d) AFM–IR absorbance map at 1604  $\text{cm}^{-1}$  showed bright white regions of higher absorbance all across the nanorod indicating the distribution of either a salt or moisture rich domain across the whole nanorod. e) Averaged AFM–IR spectra from the corresponding AFM–IR spectral array shown in (a).

had a hydrophobic apex. Furthermore, the presence of  $-\text{C}-\text{H}$  bending peak from glycolide monomer ( $\text{O}-\text{CH}_2$  and  $-\text{OH}$  peak) at 1408  $\text{cm}^{-1}$  distributed across the whole nanorod indicated the presence of higher proportion of glycolide monomer in the particle. Glycolide has been reported to have higher reactivity compared to the lactide monomer. Therefore, the content of glycolide is usually higher in the final polymeric mixture than at the beginning of the polymerization process.<sup>[24]</sup> Furthermore, the intensities of the  $-\text{C}-\text{O}$  bending band of PLGA ester (1056  $\text{cm}^{-1}$ ) and PEG ether (hydrophilic part, shoulder peak at 1120  $\text{cm}^{-1}$ ) were found to be lower at the apex of the nanorod. This indicates that the hydrophilic domains are more concentrated at the body of the nanorod. The distribution of hydrophilic and hydrophobic domains at different position of the nanorod may influence its degradation, which primarily occurs via hydrolysis after adsorption of moisture. It will also directly affect the interaction of the nanorod with proteins and biomolecules of which adsorption, distribution, and potential denaturation are associated with surface energy, charge, and size (curvature) of the particles. Our results emphasized that the AFM–IR is able to distinguish the blend of polymers in the nanorod by mapping the distribution of the monomeric units.

Such precise measurements allowed us to conclude that during the synthesis, hydrophobic ester domains preferentially assembled at both ends of the nanorod, while the hydrophilic component of PEG was distributed across the body. The presence of PEG across the nanorod highlights its potential for

drug delivery and it should be viewed positively because PEG is associated with inertness in biological environment, with poor protein adsorption, low cell activation and adhesion, and causes negligible inflammatory responses. It is well established that the modification of nanoparticles with PEG improves their biocompatibility (reduces toxicity) and increases their circulation time and biodistribution.<sup>[26]</sup> For example, bare PLGA nanoparticles induce membrane disruption leading to hemolysis of red blood cells, which can be avoided by functionalizing the nanoparticles with PEG.<sup>[26]</sup> However, in copolymers the ratio between PLGA and PEG determines the rate of loss of PEG from the PLGA–PEG composite during its degradation.<sup>[27]</sup> The higher the concentration of PEG in the copolymer blend, the greater would be the loss of PEG corresponding to faster degradation and exposure of PLGA component.<sup>[28]</sup> Subsequently, the interaction of a nanoparticle with the proteins and cell will be altered.<sup>[28]</sup> Furthermore, the specific assembly of hydrophobic and hydrophilic domains of PEG and PLGA within the nanorod contributes to variations in the charge along the particle, thus affecting its interaction with proteins (corona formation). It has been identified that the composition of the corona determines binding and internalization of the particle by cells. Therefore, knowledge of the chemical domains may allow us to predict how the nanorod “approaches” and binds to cell (Figure 5a), which is a well-recognized and deciding parameter of endocytosis.<sup>[29]</sup>

The differences in the chemical distribution evidenced by the highly spatially resolved spectra (Figure 2a) were further

confirmed by the AFM–IR maps (Figure 2b,c) collected at specific wavenumbers across the entire nanorod. When the absorbance map was collected at  $1740\text{ cm}^{-1}$  (Figure 2b) and  $1184\text{ cm}^{-1}$  (Figure 2c), “bright” regions of absorbance were seen at the peak and tail end of the nanorod (Figure 2b,c and Figure S4, Supporting Information). Whereas IR absorbance map collected at  $1604\text{ cm}^{-1}$  showed absorbance across the whole nanorod indicating the presence of either carboxylate salt or moisture across the nanorod. If a PLGA–PEG copolymer is fabricated as a diblock, then PEG chains orient themselves toward the external aqueous phase, which could contribute to the higher moisture absorbing ability of PLGA–PEG copolymer.<sup>[30]</sup> This could be the potential reason behind the appearance of the peak at  $1604\text{ cm}^{-1}$ , which is associated with moisture bound to the nanorod. Depending on the strength of the water bound to PLGA, it has been reported that the carbonyl peak can shift by 6 to  $100\text{ cm}^{-1}$  and the appearance of the peak at  $1604\text{ cm}^{-1}$  may also indicate the presence of hydrogen bonded carboxylate group in the nanorod.<sup>[25]</sup> Since it is known that both PLGA and PEG degrade at different rates, knowledge of the polymer distribution is pivotal to the design of particles with desired stiffness and degradability. Topographical images of the nanorods (Figure S4, Supporting Information) showed some deposits (rests) outside the body of the nanorods. It can be anticipated that during the fabrication some nanorods may break into smaller pieces, thus observed nanometer deposits were most likely fragments of nanorod particles. These fragments may be present in the nanorod dispersion and get deposited on the substrate during the sample preparation (Figure S6, Supporting Information). To verify that they do not form a thin layer which may interfere during the data collection from the nanorod, we collected spectra outside the nanorod and additionally from the deposits on the prism surface. The spectra collected beyond the nanorod showed that signal intensity is negligible when compared spectra collected across the nanorod. These spectra characterized with broad and flat peaks and central position of the peak suggested similar chemical composition to the nanorod particle (Figures S5 and S6, Supporting Information). Furthermore, high-resolution high images confirmed that rests were not present on the surface on nanorods and only visible in some parts of the prisms. These data gave confidence that identified distribution and location of chemical domains on the nanorod were associated purely with the material composition of the nanorod particle itself.

During the spectra acquisition with AFM–IR, simultaneously with IR signal, a contact resonance frequency can be collected. Changes to the oscillation frequency of the probe correlate with the mechanical properties of the sample. Thus, a single scan can provide detailed information about the distribution of chemical domains and qualitatively map its nanomechanical properties. The analysis of the contact resonance

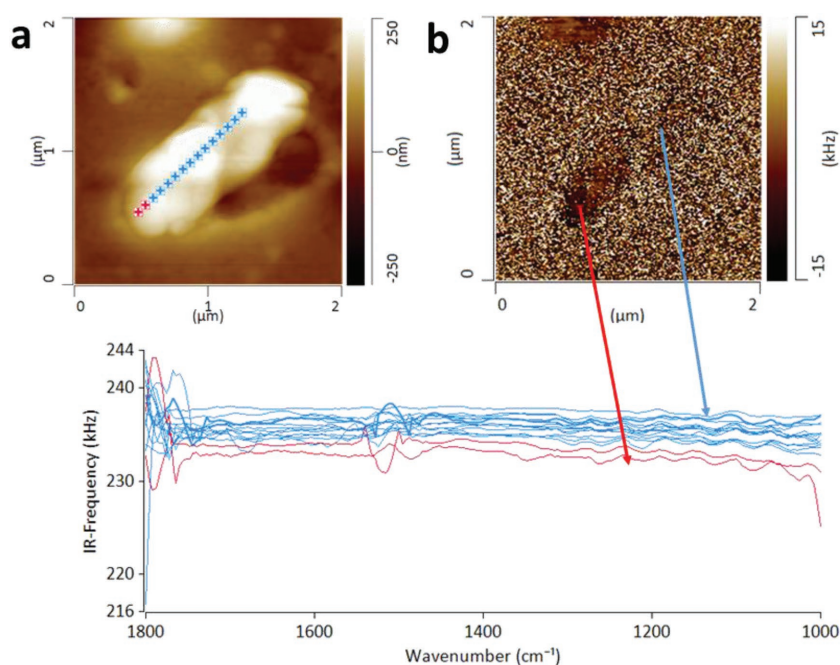


**Figure 3.** a) AFM–height image along with the AFM–IR frequency spectral array collected from the nanorod. b) AFM–IR frequency image collected at  $1604\text{ cm}^{-1}$  confirmed two distinct domain with the nanorod: (i) stiffer domains of the nanorod body (light brown regions—blue spectra) that characterize with higher contact resonance frequency and (ii) softer domains at the apex (dark brown regions—red spectra) that characterize with lower frequencies.

frequency (Figure 3a—topography and spectra) showed that there was a difference of  $\approx 6\text{ kHz}$  in the frequency between different regions across the nanorod. These regions corresponded with different chemical domains as demonstrated on the IR map collected at  $1604\text{ cm}^{-1}$ . These results demonstrated that the apex of the particle with higher ester content (dark brown region) had lower contact resonance frequency than the body of the particle indicating that these regions were “softer” than the body of the nanorod (Figure 3b). This finding was further confirmed by the LCR spectroscopy, which is an exclusive approach to probe viscoelastic properties at the nanoscale. In LCR, the contact resonance frequency corresponds to the elasticity of the sample whereas the amplitude reflects its viscosity. When LCR spectra (Figure 4a) were collected across the nanorod’s surface, the resonance frequency of the nanorod apex was on average  $118\text{ kHz}$  with an amplitude of  $0.32\text{ V}$ , whereas the body of the nanorod had the resonance frequency of  $126\text{ kHz}$  and an amplitude of  $0.26\text{ V}$ . Lower resonance frequency with higher amplitude suggested that the apex areas of the nanorods were less stiff and had lower viscosity when compared to other parts of the nanorods. This was further confirmed by the contact resonance map collected at  $118\text{ kHz}$  where regions associated with lower elasticity and lower viscosity were identified at the tip and edge of the nanorods (Figure 4b, blue color).

To differentiate between the nanomechanics, the substrate and nanorod particles spectra were collected across the particle and surrounding substrate (Figure S7, Supporting Information). Spectra collected from substrate had higher contact resonance frequency and higher amplitude than the nanorod particles

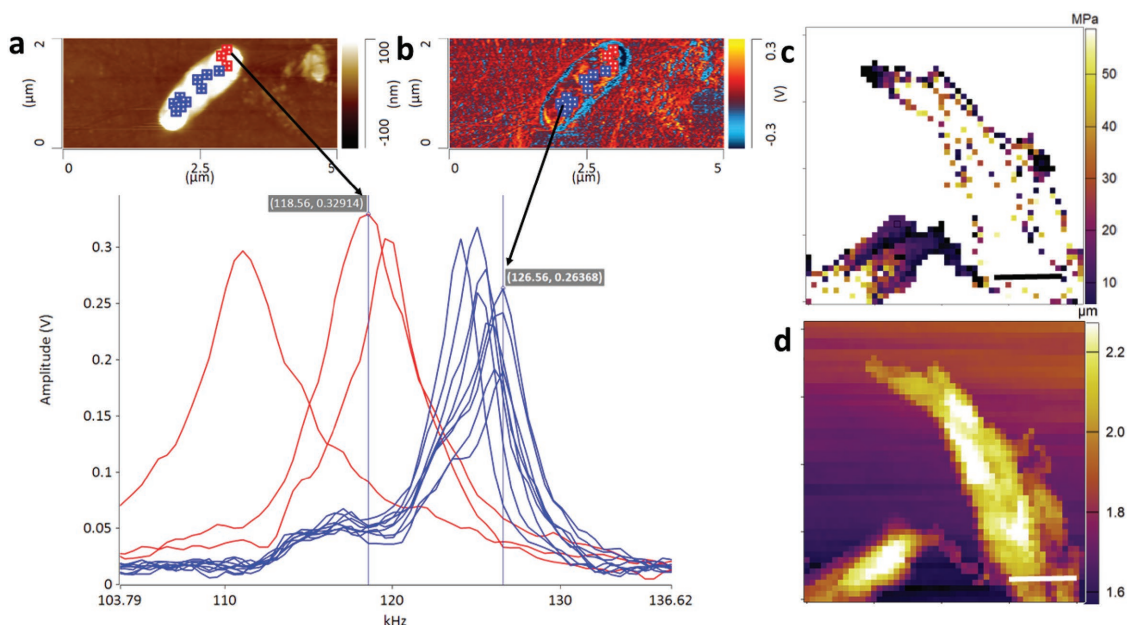


**Figure 4.** a) LCR–height image along with the contact resonance frequency spectra array collected from different position of nanorod. The apex of the nanorod had lower contact resonance frequency and higher amplitude (red marks), indicating lower stiffness and lower viscoelasticity, whereas the body of the nanorod had higher contact resonance frequency and lower amplitude demonstrating higher stiffness with higher viscoelasticity along the body of the nanorod. b) LCR contact resonance frequency image collected at 118 kHz confirmed lower stiffness at the apex of the nanorod (red marks), whereas blue marks represent the body of the nanorod with higher stiffness. c,d) Molecular force probe force map image showing the distribution of Young's modulus across the nanorod which ranged from 1.55 to 58.90 MPa, with apex and edge of the nanorod being softer (violet regions), white regions represent the stiffer body of the nanorod along with the topography image; scale bar represents 2 μm).

indicating significantly higher stiffness and lower viscoelasticity. These results also confirmed that substrate had minimal influence on the mechanical properties of the particle itself.

Variations in the viscoelasticity across the nanorod is in strong agreement with the chemical maps (Figure 2b,c,d) and confirmed the presence of interconnected network of both PLGA and PEG with local areas dominated by one of the polymers. Since stiffness of the nanoparticles modulates antibody-mediated targeting, endocytosis, and phagocytosis, detailed knowledge of mechanical properties is a prerequisite to understanding their interactions in biological systems. We know that macrophages phagocytose preferentially to rigid particles,

allowing the softer (flexible) particles to remain in blood circulation for a longer time. The use of softer particles increases the likelihood of drug delivery to the intended tissue as they are not readily phagocytosed.<sup>[31]</sup> Furthermore, it has already been demonstrated that flexible nanoparticles (flexible liposome) are endocytosed more rapidly than rigid nanoparticle (silica particles).<sup>[32]</sup> In this scenario, the number of flexible particles traversing the cell membrane would be higher (Figure 5b). In addition, the toxicity induced by nanoparticles is also dependent on their rigidity. Upon internalization of stiff rod-shaped nanoparticles, they have the potential to disrupt endosomal and lysosomal membrane, interact with mitochondria, activate

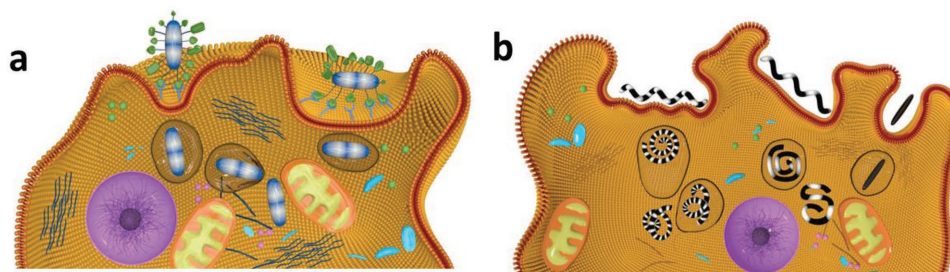


**Figure 5.** Schematic representation of variation in particle uptake depending on the nanochemistry and nanomechanics of the nanorod particles. a) Effect of chemistry on particle uptake: depending on the distribution of polymers across the particle, the type of protein or biomolecule binding at specific locations may vary and depending on whether that particle can enter in either an upright or sideways orientation. If particles are entering upright then they are taken up faster. b) Effect of mechanics on particle uptake: soft and flexible particles are endocytosed faster as they are capable of being bent and twisted by the cell on internalization. Whereas the stiffer particle may take longer to be endocytosed. The ratio of polymer components can be changed to alter the stiffness and flexibility of the particle, which will directly influence the uptake; the stiffer the particle the slower the uptake. Both the chemistry and mechanics of the nanoparticle govern its fate in the cellular environment.



Caspase-3 pathway, and damage DNA, ultimately leading to cell death and localized inflammation.<sup>[33]</sup>

Uptake of “soft” particles was shown to be faster, with viability and cell function being unaffected.<sup>[5]</sup> Therefore, producing soft, “wiggly” nanoparticles could be an effective strategy to deliver a therapeutic cargo to cells more effectively without inducing significant toxic effects.<sup>[4]</sup> The interaction of particles with cell membrane is also affected by stiffness.

For stiffer nanoparticles, adhesive interactions between the nanoparticle and membrane simply force the membrane to deform and wrap around the particle before being uptaken (Figure 5b). In contrast, softer particles initially spread on the membrane without significant membrane deformation, followed by membrane bending and progressive wrapping around the particle before being finally internalized (Figure 5b).<sup>[34]</sup>

In summary, based on previously published findings,<sup>[4,5,31–34]</sup> discussed above, it can be hypothesized that depending on the particles’ stiffness, the membrane–particle interaction may be completely different. Consequently, the internalization and toxicity of the particles can be controlled by the particles’ rigidity. This emphasizes the importance of nanomechanical assessment with the correlative atomic force microscopy presented here. To further validate our findings, we mapped the apparent elastic modulus using AFM-based force–volume measurements. By fitting Hertz’s model to the force curves collected across the entire nanorod, stiffness maps were generated (Figure 4c). The results were in strong agreement with LCR results and showed that the apparent elastic modulus ranged from 1.5 to 58.90 MPa. Similar to the AFM–IR and LCR results, we found that the apex and edge of the particle had lower apparent elastic modulus (dark brown areas), while the midsections of the nanorod (white areas) had a higher modulus. The possible explanation of higher rigidity of the nanorod in the midsection could be linked to manufacturing process. Nanorods are manufactured using the emulsion diffusion method where PLGA was dissolved in dichloromethane (DCM) which is partially miscible in the aqueous phase containing m-PEG using polyvinyl alcohol (PVA) as a surfactant. One of the most important steps in this method is solvent diffusion, in which the organic phase diffuses from the oil phase to the outer water phase leading to increased stiffness of the nanorod.<sup>[35]</sup> During the diffusion of the solvent, nonuniform crystallization of the polymers or their separation is possible and leads to the zonal distribution of the stiffness. The fact that our nanorods had lower stiffness at the tip compared to the body can be related to the absorption of moisture or formation of hydrogen bonds between the PLGA component present at the apex of these particle and water present in the environment as confirmed by the nanochemical evaluations with AFM–IR.

Despite lower resolution, force–volume measurements correlated very strongly with the results obtained using AFM–IR and LCR and provided validation of the nanomechanical results. Importantly, the results of nanomechanical properties aligned and were explained by nanostructure of the nanorod obtained using AFM–IR.

Physicochemical properties of nanomaterials are central to the development of novel technologies and since both characteristics are interrelated there is an unmet technological need to probe and resolve them in correlative manner. To address

this gap, we propose AFM-based nano-correscopy, which operates at a spatial resolution below the IR diffraction limit. The particular strength of our approach is the correlative mapping of the distribution of chemical domains across the nanoparticle, variation in viscoelasticity and apparent elastic modulus (stiffness), and even subsurface absorption of moisture. In biomedical applications, these data are pivotal to establish the mechanisms of nanoparticle interactions with biomolecules, cells (endocytosis and exocytosis), and bacteria. However, this technique is equally useful to study the structure of “biological” nanoparticles, in particular extracellular vesicles (EVs), for which morphology, chemical, and mechanical characteristics may provide a fundamental information to precisely understand their biological function. Since EVs emerged recently as a nanoscale messengers that carry key signals to (re)program cells which are also recognized as effective biomarkers of a disease, precise understanding of their nanoscale structure is crucial to use their full potential in biomedicine.<sup>[36]</sup> AFM-based techniques have already been successfully used to characterize formation and secretion of EVs.<sup>[37]</sup> Casado and co-workers<sup>[38]</sup> used AFM imaging to track the formation of bulges in living adipose tissue-derived stem cells which enabled to explain that shedding vesicles constitute a large proportion of the EV pool. Therefore, developed nano-correscopy has a significant potential to probe key physicochemical features of extracellular vesicles (EVs including exosomes and microvesicles), which underpin their biological function. The presented approach also has the power to provide insights into stability and degradation of nanoparticles. The use of such an approach is likely to provide new knowledge that will underpin the development of safe-by-design particles for biomedical applications and other fields.

Specifically, using nano-correscopy we were able to precisely identify the distribution of PLGA (monomers of lactide and glycolide) and PEG polymer across copolymer nanorods. The hydrophobic lactide component was found predominantly at the apex, while hydrophilic glycolide and PEG components assembled at the body of the nanorods. Mapping of nanomechanical properties confirmed that the nanorods had a gradient structure, which correlated with chemical composition. Mechanical properties were probed both qualitatively and quantitatively and the apparent elastic modulus ranged from 1.5 to 58.90 MPa and the distribution of stiffness correlated with the presence of each of the polymers.

## Experimental Section

**Fabrication of Nanocomposite Particles:** The rod-shaped m-PEG–PLGA nanoparticles were prepared using bulk m-PEG–PLGA copolymers with 20% PEG content (Akina, Inc. AK037). First, spherical particles were synthesized using the precipitation/solvent diffusion method.<sup>[39]</sup> Briefly, 50 mg PLGA–PEG was added to 1.25 mL of DCM, followed by 3 h of agitation for total dissolution. The polymer solution was directly added to 5 mL of 5% PVA solution. The mixture was then homogenized for 1 min using a probe sonicator to generate an oil-in-water emulsion. The formed emulsion was added to 25 mL of ice-cold deionized (DI) water and stirred for 3 h at room temperature to evaporate the DCM. Next, the particles were collected and washed three times by centrifugation at 15 500 × g at 4 °C, and passed through a 1.2 μm filter. Next, the collected nanoparticles (of mean diameter of 450 nm) were freeze dried and stored at –20 °C. To form the rod-shaped nanoparticles,

as-synthesized spherical PLGA–PEG particles were stretched into rod shape using the stretching method with slight modification.<sup>[29]</sup> In brief, 1% glycerol was added to a 10% PVA solution and spherical PLGA–PEG NPs were added to this mixture to a concentration 0.1% w/v. Fifteen milliliters of the solution was dried on a 12 cm × 16 cm flat surface to form an 80 μm thick film. The film was cut into sections, and then stretched in one direction at a temperature above 70 °C using a custom-made apparatus. The stretched films were dissolved in DI water. Obtained nanoparticles were washed by centrifugation at 12 000 × g with the DI water at least five times to remove PVA from the surface of the nanoparticles. Purified nanoparticles were freeze dried, weighed, and stored at –20 °C for further use.

**Nanoscale Chemical Analysis—AFM–IR—Sample Preparation:** The freeze dried particles were redispersed in DI water with gentle vortex. Ten microliters of dispersed particles were transferred to a zinc selenide prism and dried under nitrogen gas. The sample was stored in a desiccator to remove the adsorbed moisture prior to AFM–IR spectral acquisitions.

**Nanoscale Chemical Analysis—AFM–IR—Physicochemical Analysis:** To investigate the distribution of copolymers across the nanoparticles, nanoscale chemical analysis was carried out using a nanoIR AFM–IR instrument (Anasys Instruments, USA). Prior to the acquisition of the spectra, four IR background spectra were collected from 1000 to 1800 cm<sup>–1</sup>. These spectra were averaged and normalized to calibrate the signal intensity as a function of wavenumber. The second cantilever oscillation mode was chosen to optimize the cantilever ringdown signal at the frequency center of 238 kHz using a frequency window of 50 kHz. The infrared laser focus was optimized at 1050, 1190, 1390, 1600, and 1730 cm<sup>–1</sup>. Coaverages of 256 scans were used for optimization. The laser power was adjusted to obtain a clean and distinct “IR-hotspot” in the center of the image, which corresponded to the location, where the AFM tip was in contact with the sample (Figure S1, Supporting Information). The AFM–IR spectra were collected from 1000 to 1800 cm<sup>–1</sup> at 4 cm<sup>–1</sup> intervals, coaveraging a total of 256 cantilever ringdown signals at each wavenumber. The laser source produced 10 ns pulses at a repetition rate of 1 kHz. The spectral resolution was determined by the laser line width and was estimated to be 8 cm<sup>–1</sup> in this spectral range. A minimum of 10 to 12 spectra were collected across the particle with a step size of 150 nm. The spectra were presented either as an array of spectra to show spatial locations (Figure 2a, Figures S4–S6, Supporting Information) or were averaged and plotted for analysis, as in the case of Figure 2c and Figure S4e (Supporting Information). IR maps of the samples were collected in contact mode at a scan rate of 0.1 Hz at a resolution of 500 × 256 points with 16 coaverages using an uncoated silicon nitride cantilever with a nominal spring constant of 0.5 N m<sup>–1</sup> (EXC450 tips, AppNano, CA, USA). Minimum of 10 to 12 particles were analyzed and the results presented were representative samples. All spectral analyses were undertaken using Analysis Studio software (Anasys Instruments, USA), smoothing being achieved with a Savitzky–Golay third-order polynomial function on 5 points.

**Nanoscale Chemical Analysis—AFM–IR—Nanomechanical Analysis of Viscoelastic Properties of Nanoparticles—Lorentz Contact Resonance Spectroscopy:** The particles deposited on zinc selenide prisms were imaged using the nanoIR instrument equipped with ThermoLever cantilever with a spring constant of 0.1–0.5 N m<sup>–1</sup>, resonant frequency of 15–30 kHz, and tip radius of <30 nm (AnasysInstruments, USA) operating in LCR mode. LCR spectra which provide detailed information of viscous and elastic properties of the substrate were collected across the particles by sweeping over the drive frequency range of 1 to 1000 kHz at an increment rate of 100 kHz s<sup>–1</sup>. LCR images representing the distribution of viscoelasticity were obtained by locking the resonance frequency of the cantilever specific to a contact resonance frequency of one of the materials.

**Nanoscale Chemical Analysis—AFM–IR—Molecular Force Probe Spectroscopy:** To investigate the stiffness distribution, nanorods were probed using Molecular Force Probe (MFP-3D-Bio, Asylum Research, USA) operating in force–volume mode and using a silicon nitride cantilever with reflex side gold coating with a nominal spring constant of 0.049 N m<sup>–1</sup> (HYDRA-ALL-G-50, AppNano, CA, USA). Nanorods were

dispersed in 1× phosphate buffered saline (PBS) and were transferred to 50 mm × 9 mm Petri dish (Bacteriological petri dish, Falcon, Corning, USA). These nanorods were allowed to settle at the bottom of the dishes for 1 h followed by washing with PBS 3× to remove unattached particles before carrying out the measurements. The measurements were done in 1× PBS prewarmed at 37 °C and the temperature was maintained using a heated stage, regular monitoring of the temperature was done to ensure the temperature remained within ±2 °C. To determine the stiffness distribution of nanorods (stiffness map), 400 points were indented/measured for each sample. Stiffness of particles represented by the apparent elastic modulus ( $E^*$ ) was calculated using the Hertz model using a Poisson's ratio of 0.33.<sup>[40]</sup> To obtain the stiffness maps, the nanorods were first located using a light microscope and then imaged in contact mode using silicon nitride probes. Prior to the measurements, the spring constant of each probe was determined using the thermal method and determined to be ≈65 pN N m<sup>–1</sup>. Next, the probe was lowered at a speed of 2.64 μm s<sup>–1</sup> onto the nanorods and pressed until the threshold force of 20 nN was reached. The deflection of the cantilever was plotted against the displacement in the z-direction, which gave the force–distance curves. Apparent elastic modulus was calculated from the individual curves, which consequently provided maps of stiffness. These maps represented the variation of apparent elastic modulus across nanoparticles' surface.

## Supporting Information

Supporting Information is available from the Wiley Online Library or from the author.

## Acknowledgements

The authors acknowledge Australian Institute for Nanoscale Science and Technology, The University of Sydney for providing funding (AINST Accelerator Scheme). D.K. is a recipient of an Australian Leadership Award scholarship. Authors acknowledge Surendra Prajapati for his help with graphical illustrations drawing.

## Conflict of Interest

The authors declare no conflict of interest.

## Keywords

atomic force microscopy, Lorentz contact resonance spectroscopy, molecular force probe microscopy, nanocharacterization, nano-infrared spectroscopy

Received: November 9, 2017

Revised: February 12, 2018

Published online: April 3, 2018

- [1] M. Müllner, *Macromol. Chem. Phys.* **2016**, 217, 2209.
- [2] A. C. Anselmo, S. Mitragotri, *Adv. Drug Delivery Rev.* **2017**, 108, 51.
- [3] E. Hinde, K. Thammairaphop, H. T. Duong, J. Yeow, B. Karagoz, C. Boyer, J. J. Gooding, K. Gaus, *Nat. Nanotechnol.* **2017**, 12, 819.
- [4] A. Garapaty, J. A. Champion, *Bioeng. Transl. Med.* **2017**, 2, 92.
- [5] W. Liu, X. Zhou, Z. Mao, D. Yu, B. Wang, C. Gao, *Soft Matter* **2012**, 8, 9235.



- [6] D. Bennet, S. Kim, in *Application of Nanotechnology in Drug Delivery* (Ed: A. D. Sezer), InTech, Rijeka, Croatia **2014**, Ch. 8.
- [7] P. Rivera Gil, G. Oberdörster, A. Elder, V. Puentes, W. J. Parak, *ACS Nano* **2010**, *4*, 5527.
- [8] D. R. Baer, D. J. Gaspar, P. Nachimuthu, S. D. Techane, D. G. Castner, *Anal. Bioanal. Chem.* **2010**, *396*, 983.
- [9] A. Downes, R. Mouras, A. Elfick, *J. Biomed. Biotechnol.* **2010**, *2010*, 101864.
- [10] W. Fu, W. Zhang, *Small* **2017**, *13*, 1603525.
- [11] A. Dazzi, C. B. Prater, *Chem. Rev.* **2016**, *117*, 5146.
- [12] A. Dazzi, C. B. Prater, Q. Hu, D. B. Chase, J. F. Rabolt, C. Marcott, *Appl. Spectrosc.* **2012**, *66*, 1365.
- [13] D. Khanal, A. Kondyurin, H. Hau, J. C. Knowles, O. Levinson, I. Ramzan, D. Fu, C. Marcott, W. Chrzanowski, *Anal. Chem.* **2016**, *88*, 7530.
- [14] G. Dan, X. Guoxin, L. Jianbin, *J. Phys. D: Appl. Phys.* **2014**, *47*, 013001.
- [15] D. Khanal, E. Dillon, H. Hau, D. Fu, I. Ramzan, W. Chrzanowski, *J. Mater. Sci.: Mater. Med.* **2015**, *26*, 272.
- [16] N. Hurduc, B. C. Donose, A. Macovei, C. Paius, C. Ibanescu, D. Scutaru, M. Hamel, N. Branza-Nichita, L. Rocha, *Soft Matter* **2014**, *10*, 4640.
- [17] R. Proksch, S. Kalinin, *PFM App Note* **2008**.
- [18] U. Rabe, in *Applied Scanning Probe Methods II: Scanning Probe Microscopy Techniques* (Eds: B. Bhushan, H. Fuchs), Springer, Berlin **2006**, pp. 37–90.
- [19] N. Li, C. J. Gilpin, L. S. Taylor, *Mol. Pharmaceutics* **2017**, *14*, 1691.
- [20] D. Khanal, H. Hau, A. Kondyurin, D. Fu, I. Ramzan, W. Chrzanowski, *Int. J. Nanotechnol.* **2017**, *14*, 133.
- [21] E. Dillon, K. Kjoller, C. Prater, *Microsc. Today* **2013**, *21*, 18.
- [22] C. Marcott, M. Lo, E. Dillon, K. Kjoller, C. Prater, *Microsc. Today* **2015**, *23*, 38.
- [23] M. Portaccio, C. Menale, N. Diano, C. Serri, D. G. Mita, M. Lepore, *J. Appl. Polym. Sci.* **2015**, *132*, 41305.
- [24] C. D. A. C. Erbetta, R. J. Alves, J. M. Resende, R. F. de Souza Freitas, R. G. de Sousa, *J. Biomater. Nanobiotechnol.* **2012**, *3*, 208.
- [25] B. Jeong, C. F. Windisch, M. J. Park, Y. S. Sohn, A. Gutowska, K. Char, *J. Phys. Chem. B* **2003**, *107*, 10032.
- [26] D. Kim, H. El-Shall, D. Dennis, T. Morey, *Colloids Surf., B* **2005**, *40*, 83.
- [27] K. Avgoustakis, A. Beletsi, Z. Panagi, P. Klepetsanis, A. G. Karydas, D. S. Ithakissios, *J. Controlled Release* **2002**, *79*, 123.
- [28] A. Beletsi, Z. Panagi, K. Avgoustakis, *Int. J. Pharm.* **2005**, *298*, 233.
- [29] J. A. Champion, S. Mitragotri, *Proc. Natl. Acad. Sci. USA* **2006**, *103*, 4930.
- [30] H. K. Makadia, S. J. Siegel, *Polymers* **2011**, *3*, 1377.
- [31] R. Toy, K. Roy, *Bioeng. Transl. Med.* **2016**, *1*, 47.
- [32] W. C. Huang, P. A. Burnouf, Y. C. Su, B. M. Chen, K. H. Chuang, C. W. Lee, P. K. Wei, T. L. Cheng, S. R. Roffler, *ACS Nano* **2016**, *10*, 648.
- [33] B. Zhang, P. Sai Lung, S. Zhao, Z. Chu, W. Chrzanowski, Q. Li, *Sci. Rep.* **2017**, *7*, 7315.
- [34] X. Yi, X. Shi, H. Gao, *Phys. Rev. Lett.* **2011**, *107*, 098101.
- [35] Y. Wang, P. Li, T. Truong-Dinh Tran, J. Zhang, L. Kong, *Nanomaterials* **2016**, *6*, 26.
- [36] I. M. Bjorge, S. Y. Kim, J. F. Mano, B. Kalionis, W. Chrzanowski, *Biomater. Sci.* **2018**, *6*, 60.
- [37] S. Casado, M. d. V. T. Lobo, C. L. Paíno, *Sci. Rep.* **2017**, *7*, 6767.
- [38] C. L. Paíno, S. Casado, *Hum. Gene Ther.* **2013**, *24*, A69.
- [39] P. Xu, E. Gullotti, L. Tong, C. B. Highley, D. R. Errabelli, T. Hasan, J.-X. Cheng, D. S. Kohane, Y. Yeo, *Mol. Pharmaceutics* **2008**, *6*, 190.
- [40] H. Hertz, *J. Reine Angew. Math.* **1881**, *92*, 156.